Molecular beam epitaxy growth of axion insulator candidate $EuIn_2As_2$

Muhsin Abdul Karim,[1,*] Jiashu Wang,[1,*] David Graf,[2] Kota Yoshimura,[1] Sara Bey,[1] Tatyana Orlova,[3] Maksym Zhukovskyi,[3] Xinyu Liu, and Badih A. Assaf[1,†]

[1]*Department of Physics and Astronomy, University of Notre Dame, Notre Dame, Indiana 46556, USA*
[2]*National High Magnetic Fields Laboratory, Florida State University, Tallahassee, Florida 32310, USA*
[3]*Notre Dame Integrated Imaging Facility, University of Notre Dame, Notre Dame, Indiana 46556, USA*

(Received 29 June 2023; accepted 11 September 2023; published 9 October 2023)

The synthesis of thin films of magnetic topological materials is necessary to achieve novel quantized Hall effects and electrodynamic responses. $EuIn_2As_2$ is a recently predicted topological axion insulator that has an antiferromagnetic ground state and an inverted band structure, but has only been synthesized and studied as a single crystal. We report on the synthesis of *c*-axis-oriented $EuIn_2As_2$ films on sapphire substrates by molecular beam epitaxy. By carefully tuning the substrate temperature during growth, we stabilize the Zintl phase of $EuIn_2As_2$ expected to be topologically nontrivial. The magnetic properties of these films reproduce those seen in single crystals, but their resistivity is enhanced when grown at lower temperatures. We additionally find that the magnetoresistance of $EuIn_2As_2$ is negative even up to fields as high as 31 T. While it is highly anisotropic at low fields, it becomes nearly isotropic at high magnetic fields above 5 T. Overall, the transport characteristics of $EuIn_2As_2$ appear similar to those of chalcogenide topological insulators, motivating the development of devices to gate tune the Fermi energy and reveal topological features in quantum transport.

DOI: 10.1103/PhysRevMaterials.7.104202

I. INTRODUCTION

Magnetic topological insulators with a ferromagnetic ground state are behind the recent discovery of the quantized Hall effect at zero magnetic field [1]. This discovery has since stimulated a search for topological materials that host complex magnetic ground states beyond ferromagnetism, which can lead to other interesting and technologically relevant topological phases [2–5].

$EuIn_2As_2$ is a candidate material that falls in this category. It has a layered crystal structure consisting of alternating europium and In_2As_2 planes stacked along its *c*-axis [6]. It exhibits antiferromagnetic order at low temperature, resulting from the interaction between europium atoms occupying neighboring layers. Our primary motivation to study this material comes from theoretical predictions that $EuIn_2As_2$ is an axion insulator with a zero Chern number and a quantized magnetoelectric coupling term. The axion insulator state results from a band inversion in a crystal with inversion symmetry that hosts antiferromagnetism that breaks time-reversal symmetry [7]. These predictions argue that $EuIn_2As_2$ is the first stoichiometric compound with intrinsic magnetic order to belong to this topological class. Magnetometry measurements of $EuIn_2As_2$ single crystals show the presence of an antiferromagnetic ordering at low temperatures with an in-plane magnetic easy axis [8]. More recently, neutron diffraction measurements reported observing a helical magnetic structure, challenging the prior belief that $EuIn_2As_2$ has a collinear magnetic ordering [9]. The topological axion phase predicted by Ref. [7] is altered when the ground state is helimagnetic, but the topological character of the material was argued to be preserved [9]. Experimental evidence of a band inversion in $EuIn_2As_2$ from angle-resolved photoemission spectroscopy measurements makes this material a very good candidate to search for novel physics stemming from coexisting topological and magnetic order [10,11].

The electrical transport properties of $EuIn_2As_2$ have also been studied in the past [6,8,12–15]. The material exhibits a peak in the resistivity at the Néel temperature followed by a drop at low temperature. $EuIn_2As_2$ also exhibits a negative magnetoresistance (MR), common to many europium-based antiferromagnets, including EuB_6, $EuIn_2P_2$, and (Eu,Gd)Se [16–18]. It is maximized at the Néel temperature but is maintained in the ordered state [6].

All of the previously mentioned studies on the structural, magnetic, and electrical properties of $EuIn_2As_2$ were conducted on single crystals. Without a doubt, there is a need for thin films of this material to probe magnetotransport signatures of predicted topological edge or surface states [7,9], as well as the magnetoelectric responses [19,20] potentially due to its quantized axion angle. Thin films would also enable the realization of gated Hall bars of this material needed to gate tune the Fermi energy, typically located in the valence band, into the bulk gap [10]. Without this, the native doping observed in previous studies would mask the contribution of topological edge or surface states [10]. $EuIn_2As_2$ cannot be mechanically exfoliated, so the development of its synthesis by molecular beam epitaxy (MBE) is needed. This problem is challenging because the Zintl phase of $EuIn_2As_2$ competes with the highly studied and thermodynamically favorable

*These authors contributed equally to this work.
†bassaf@nd.edu

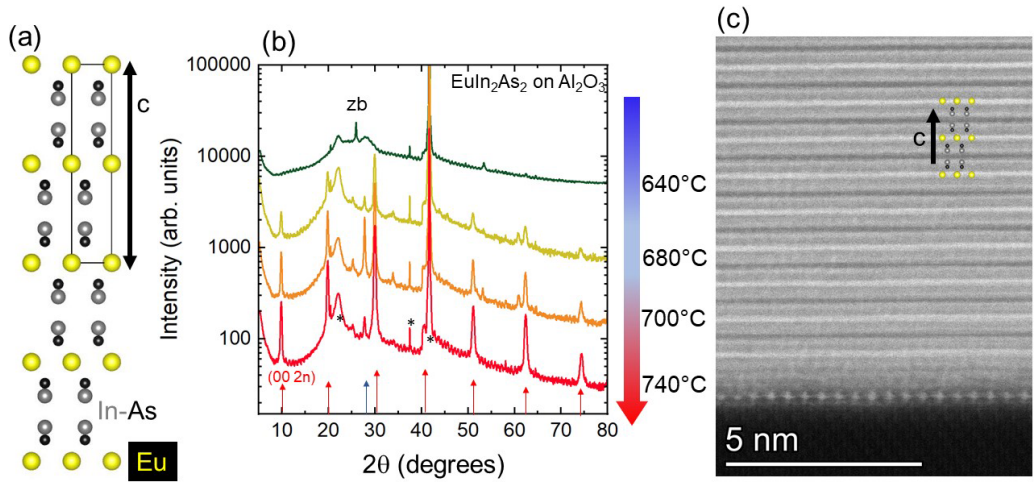

FIG. 1. (a) Crystal structure of $EuIn_2As_2$. (b) X-ray diffraction patterns measured on a series of Eu-In-As films grown on sapphire between 640°C and 740 °C. The $(0\,0\,2n)$ Bragg series of $EuIn_2As_2$ is highlighted by red arrows. The (111) Bragg peak of the zincblende structure is labeled zb and is seen clearly in the sample grown at 640 °C. The * symbol marks the Bragg peaks of the sapphire substrate and instrument artifacts. The blue arrow denotes the position of the (102) Bragg peak of $EuIn_2As_2$. (c) High-angle annular dark-field scanning TEM image of a sample grown at 740 °C. The films grown at 740 °C and 680 °C are 45 nm thick; the one grown at 700 °C is 75 nm.

zincblende arsenide phases at low substrate growth temperatures.

In this work, we overcome this challenge and successfully identify a temperature region in the MBE growth scheme at which the Zintl phase becomes thermodynamically favorable, yielding a layered $EuIn_2As_2$ structure. The onset of this phase occurs at a substrate temperature of 680 °C, well above the ideal growth window of InAs. Using this developed growth scheme, we achieve $EuIn_2As_2$ films on (0001)-oriented Al_2O_3, which are 45 to 100 nm thick, and reproduce the magnetic properties seen in bulk single crystals. The resistivity in our samples is likely controlled by film morphology, as it is consistently larger than the resistivity in single crystals. We also observe a negative magnetoresistance consistent with the magnetic polaron picture, resulting from scattering due to magnetic fluctuations. Its anisotropy follows the magnetic anisotropy of the crystal at low magnetic fields, but is suppressed at high magnetic fields despite remaining negative all the way up to 31 T.

II. RESULTS

A. Molecular beam epitaxy and characterization

MBE growth of $EuIn_2As_2$ films is carried out on (0001)-oriented sapphire substrates. We chose sapphire ($a = 4.758$ Å) because of its ability to withstand high substrate temperatures, despite its lattice mismatch with $EuIn_2As_2$ ($a = 4.21$ Å). The temperatures of elemental sources are tuned to ensure beam-equivalent pressures (BEPs) that maintain arsenic-rich conditions through the growth. The As:Eu BEP ratio is between 20:1 and 29:1, while the As:In BEP ratio is kept close to 10:1. Indium and arsenic (both 99.9999% pure) and europium (99.99% pure) are evaporated from standard Knudsen cells. The base pressure in the MBE is 5×10^{-9} torr. The substrate temperature T_{sub} is varied between 640 and 740 °C. As we shall show next, as T_{sub} approaches the indium cell temperature, exceeding that of europium and arsenic, the nucleation of elemental layers and zincblende phases is suppressed. Under these conditions, the Zintl phase is formed. Also, it is worth highlighting that T_{sub} is significantly higher than what is commonly used for III-V zincblende materials. This requirement also motivates our substrate choice, since sapphire is known to remain structurally stable at these temperatures, unlike III-V semiconductor wafers [21].

X-ray diffraction measurements are carried out using a copper $K\alpha$ source in the specular direction on films grown at various T_{sub}. They yield the patterns shown in Fig. 1(b). At 640 °C, the nucleation of InAs (possible europium doped) is thermodynamically favored and is evidenced by the peak highlighted by the gray arrow close to $2\theta = 25°$. As of $T_{sub} =$ 680 °C, a periodic pattern of peaks repeating almost every 10° emerges and grows stronger as temperature increases to 740 °C. These Bragg peaks are characteristic of the layered c-axis-oriented Zintl phase of $EuIn_2As_2$ shown in Fig. 1(a) and agree with what has been previously reported [6,8,9]. From this pattern, we find a lattice constant $c = 17.874 \pm 0.003$ Å (see analysis in the Appendix). It is 0.1% larger than what is reported by Zhang *et al.* [8], 0.7% larger than what is found by Riberolles *et al.* [9], but 0.08% smaller than what is found by Goforth *et al.* [6] in single crystals. It is within sample-to-sample variations seen in single crystals. For films grown at lower substrate temperatures, an additional Bragg peak matching the (102) $EuIn_2As_2$ Bragg line can be seen below 30°. It is, however, dramatically weaker than the $EuIn_2As_2$ (006) for the film grown at 740 °C. Thus, with the appropriately tuned substrate temperature, we synthesize dominantly c-axis-oriented $EuIn_2As_2$ films on sapphire despite the large lattice mismatch between the in-plane lattice parameters of the two materials.

Cross-sectional transmission electron microscopy images were acquired using a double-tilt holder and probe-corrected Spectra 30-300 transmission electron microscope (Thermo Fisher Scientific, USA) equipped with a field emission gun

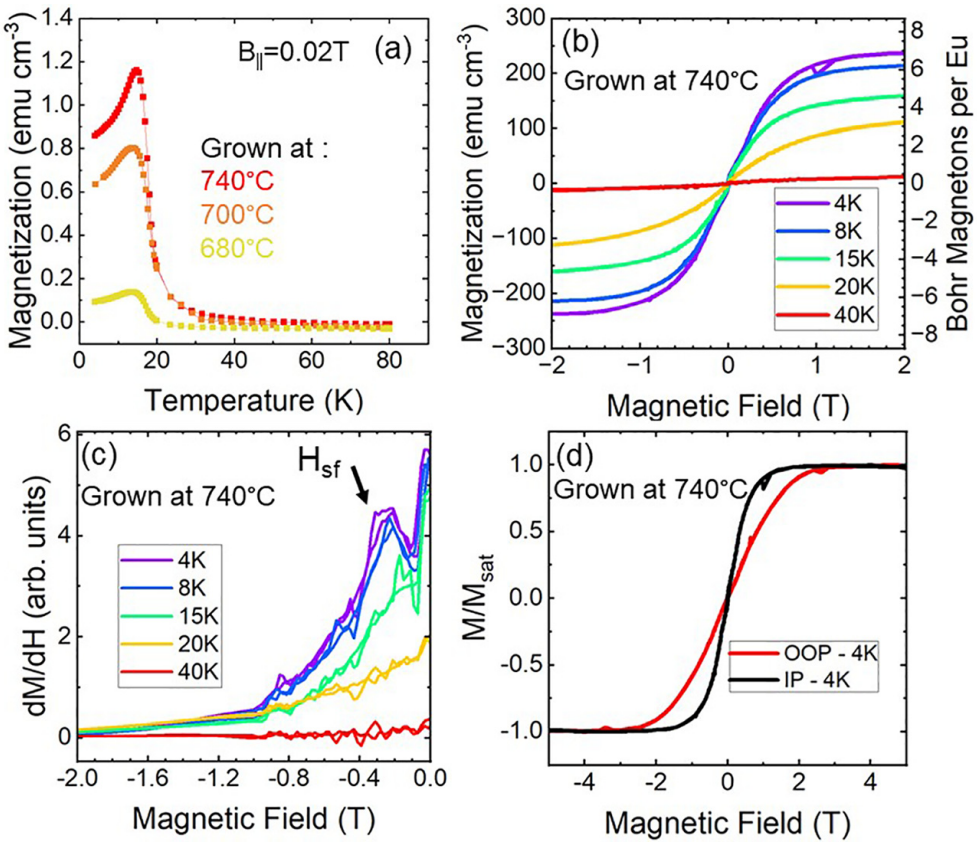

FIG. 2. (a) Magnetization versus temperature for the three samples grown above 680 °C. (b) Magnetization versus temperature for the sample grown at 740 °C measured at $B = 0.02$ T applied in plane. (c) Derivative of the magnetization with respect to magnetic field from the curves shown in (b). H_{sf}: spin-flop field. (d) Magnetization divided by its saturation plotted versus magnetic field applied out of plane (OOP) and in plane (IP).

operated at 300 kV. The TEM image in Fig. 1(c) confirms the layered Zintl phase with a c lattice constant close to 18 Å, consistent with x-ray diffraction. An amorphous layer is seen near the interface, but its thickness does not exceed a single unit cell. Energy dispersive x-ray spectra acquired during these measurements yield the composition of the layer $Eu_{(1.05\pm0.10)}In_{(1.90\pm0.15)}As_{(2.05\pm0.10)}$.

B. Magnetic properties

Superconducting quantum interference device magnetometry measurements are performed next using a Quantum Design MPMS-5 system. They reveal properties expected for $EuIn_2As_2$ and are consistent with previous studies on single crystals [6,8,12,13,15]. Figure 2(a) shows temperature-dependent measurements of the magnetization of the three films grown above 680 °C down to $T = 5$ K. A peak is systematically seen at 14 K, but is preceded by the onset magnetic order slightly below 20 K, close to the Néel temperature reported in single crystals (17 K) [6,8,15,22]. The field-dependent magnetization is also measured in all samples that contain the Zintl phase. We focus on the sample grown at 740 °C, which shows the highest purity, but we note that the film grown at 700 °C exhibits comparable properties. Figure 2(b) plots the magnetization as a function of the magnetic field applied in the ab plane of the film. It is evident from this plot that $EuIn_2As_2$ exits the antiferromagnetic ground state at low magnetic field. By 2 T, the system is saturated to a ferromagnetic state, with a saturation value close to 6.8 μ_B/Eu. We note that in this film, we also observe a small remanent magnetization of 0.3 μ_B/Eu, likely due to an unpaired europium layer at the surface. The first derivative of the $M(H)$ curves is plotted in Fig. 2(c), highlighting a peak at 0.3 T. It corresponds to the spin-flop transition of the system when the magnetic field is applied along the easy axis. In Fig. 2(d), we plot the magnetization measured with the field applied along two perpendicular directions, in-plane and out-of-plane, at 4 K. The magnetization saturates faster in the in-plane direction, confirming in-plane anisotropy, consistent with a (001)-oriented $EuIn_2As_2$ film, with its c-axis along the growth direction.

Table I compares the magnetic properties of the sample grown at 740 °C to those measured in single crystals. The saturation magnetization per europium and the saturation field in the out-of-plane direction agree with previous findings. The spin-flop field extracted from dM/dH is found to be larger [8,13,15]. However, the observed spin-flop peak in dM/dH is somewhat broad (±0.05 T at half maximum). The spin-flop transition in antiferromagnets is determined by the competition between the magnetic exchange and anisotropy energy [23–25], so that

$$H_{sf} = \sqrt{(H_A)(2H_E - H_A)}.$$

The anisotropy (H_A) and exchange magnetic (H_E) fields can be determined by comparing the in-plane ($B_{sat}^{IP} = 1.3$ T)

TABLE I. Magnetic sample characteristics compared to those from single crystals.

Source	$M_{sat}(\mu_B/\text{Eu})$	B_{sat}^{OOP} (T)	B_{sf} (T)
This work ($t = 45$ nm, 740 °C)	6.8	2.3	0.25 ± 0.05 (4 K)
Ref. [15]	6.9	2	0.21 (2 K)
Ref. [6]	7.378	2	–
Ref. [13]	6.7	2	0.21 (10 K)
Ref. [12]	6.9	1.7	–
Ref. [8]	6.9	1.9	0.19 (2 K)

and out-of-plane ($B_{sat}^{OOP} = 2.3$ T) saturation fields [Fig. 2(c)] [8],

$$\mu_0 H_E = \frac{B_{sat}^{OOP} + B_{sat}^{IP}}{4} \quad \text{and} \quad \mu_0 H_A = \frac{B_{sat}^{OOP} - B_{sat}^{IP}}{2}.$$

We find $\mu_0 H_E \approx 0.9$ T and $\mu_0 H_A \approx 0.5$ T. From that we can determine $\mu_0 H_{sf} \approx 0.8$ T, which is inconsistent with experimental findings, as also seen in Ref. [8]. This inconsistency implies that the spin-flop transition cannot be accounted for by a molecular field treatment that simply includes nearest-neighbor exchange interactions and magnetic anisotropy. There must be competing exchange interactions influencing H_{sf}. Ref. [9] has found a broken helimagnetic state in $EuIn_2As_2$ at low temperature. But, so far, no work has reported a theoretical treatment computing the phase diagram of the material with the interactions responsible for the broken helix included. Those interactions could account for the spin-flop transition occurring at such a low magnetic field. In our case, the broadening of the transition and the slight enhancement of the saturation fields are due to the film morphology. We discuss this later.

C. Magnetotransport measurements

Magnetotransport measurements are carried out using a Quantum Design MPMS5 on the film exhibiting the Zintl phase and grown at 740 °C. A magnetic field up to 7 T is applied along the c-axis, and the measurements are carried out down to 4 K. The measured sample is rectangular and is connected in a Hall configuration. The Hall resistance is first shown in Fig. 3(a) for different temperatures. It is robustly linear at a high magnetic field above 2 T, but exhibits a nonlinearity at low field. The charge carrier density extracted from the Hall slope is found to be 7.5×10^{19} holes/cm^3, comparable with what is typically found in topological insulators such as uncompensated Bi_2Te_3 [26–28] and with previous work on single crystals of $EuIn_2As_2$ [10,12]. Subtracting the slope of the normal Hall effect reveals an anomalous Hall component [shown in Fig. 3(b)]. It does not exceed 0.55 Ω at saturation. This value corresponds to a two-dimensional Hall conductivity of $0.2e^2/h$ evidencing a strong anomalous Hall effect. Qualitatively, the anomalous Hall resistance has the same field dependence as the magnetization [Fig. 2(d)], both saturating at 2 T when the field is applied along the c-axis. The Hall resistivity reaches 2.5 $\mu\Omega$-cm at saturation, comparable to what is found in single crystals [12]. In Ref. [12], a nonmonotonic Hall resistivity versus magnetic field, referred to as a topological Hall effect, is observed and is attributed to the noncoplanar spin texture of $EuIn_2As_2$. We do not see evidence of such a behavior in our films.

The temperature dependence of the resistivity is shown in Fig. 3(c). A prominent peak occurs at 18 K, consistent with the Néel temperature of $EuIn_2As_2$, and is followed by a drop in resistivity when the material enters its ordered magnetic ground state. This behavior is qualitatively consistent with what was seen in $EuIn_2As_2$ single crystals [6,12,15] and many other europium-based compounds, regardless of topological character [17,18,29–31]. The drop is enhanced with increasing magnetic field, demonstrating an enhancement of the conductivity with increasing ferromagnetic saturation. The magnetoresistance of this sample is shown in Fig. 3(d). It is consistently negative up to 7 T. This behavior was discussed in previous work on $EuIn_2As_2$ and $EuIn_2P_2$ [6,32,33], and is thought to be a result of magnetic fluctuations that get suppressed by the applied magnetic field above the magnetic ordering temperature. A similar behavior occurs when transport is dominated by hopping between magnetic polaron clusters, and is suggested to happen in EuO [29], (Eu,Gd)Se [17], EuB_6 [18,30,31], manganites [34], and other europium-based Zintl compounds [32,35].

To understand this behavior further, the MR is plotted as a function of magnetization relative to its saturation $m = M/M_{sat}$ in Fig. 4(a). The low-field MR clearly varies as $\text{MR} = Cm^2$, consistent with the Majumdar-Littlewood relation. This ties the MR's behavior to the role of magnetic fluctuations and their suppression at high magnetic field [34]. From the Majumdar-Littlewood relation, we can relate C to the charge carrier density and correlation length ξ_0 between fluctuating spins:

$$C = \left(\tfrac{1}{2} k_f \xi_0\right)^2 = \tfrac{1}{4}(3\pi^2 n)^{2/3} \xi_0^2.$$

Here, k_f is the Fermi wavevector and $n = \frac{k_f^3}{3\pi^2}$ is the charge carrier density. The expression of n in terms of k_f assumes a spherical Fermi surface. The three-dimensional shape of the Fermi surface of $EuIn_2As_2$ is unknown, so our assumption only gives an effective k_f. In the diffusive regime, this choice of effective k_f is more suitable than the assumption that $k_{||} = k_f$ [8]. With this assumption, we recover a correlation length of 11 Å at 20 K, close to the out-of-plane lattice constant and to the separation between the europium planes.

The negative MR persists at low temperatures, well below the Néel temperature. Its anisotropy further correlates with the behavior of the magnetization below the Néel temperature. We have measured its angular dependence up to 31 T at 1.6 K. These data are shown in Fig. 4(b). A large cusp is observed between ±5 T. The cusp is broader when the field is applied along the c-axis [Fig. 4(b), inset], perpendicular to the magnetic easy axis of $EuIn_2As_2$. This confirms the MR

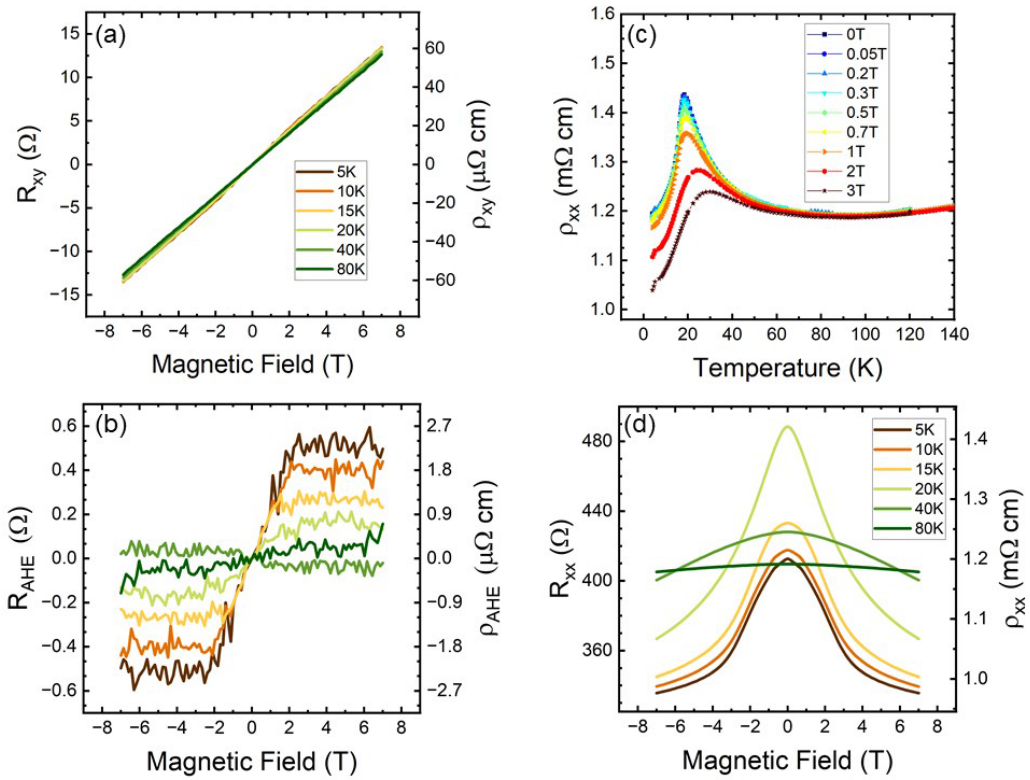

FIG. 3. (a) Hall resistance R_{xy} of the 45-nm $EuIn_2As_2$ film grown at $T_{sub} = 740\,^{\circ}C$ measured up to 7 T between 5 K and 80 K. (b) Anomalous part of the Hall effect obtained for different temperatures after subtracting a linear slope from R_{xy} at high magnetic field. (c) Resistivity of the same $EuIn_2As_2$ film versus temperature at different applied magnetic fields from 0 to 3 T. (d) Resistance R_{xx} as a function of applied magnetic field up to 7 T.

saturates more slowly along the hard axis and correlates it with the amount of the magnetic field that it takes to saturate the magnetization. This finding is consistent with the magnetic polaron picture even below the Néel temperature. At very high magnetic fields well above 2 T and up to 31 T, the MR remains negative, despite the magnetization saturating, but becomes nearly isotropic. In Fig. 4(c), we see evidence of this as the MR has a strong angular dependence at 1 T and 2 T, but is nearly independent of angle at 5 T and above. A likely contribution to the MR at very high magnetic fields could come from the spin-Zeeman and cyclotron energy altering the band dispersion of $EuIn_2As_2$. This band origin of the negative MR has been studied in the past, both in the extreme quantum limit and in the diffusive limit [36,37]. However, a good knowledge of the shape of the bulk Fermi surface of $EuIn_2As_2$ is required to tie the negative MR conclusively to a band origin.

The finding of negative MR originating from polaron hopping at low magnetic field is not unexpected for a europium-containing semiconductor. However, the MR and its anisotropy are striking evidence that bulk states dominate magnetotransport signatures in this material. We must highlight that these bulk states clearly yield a magnetoresistance

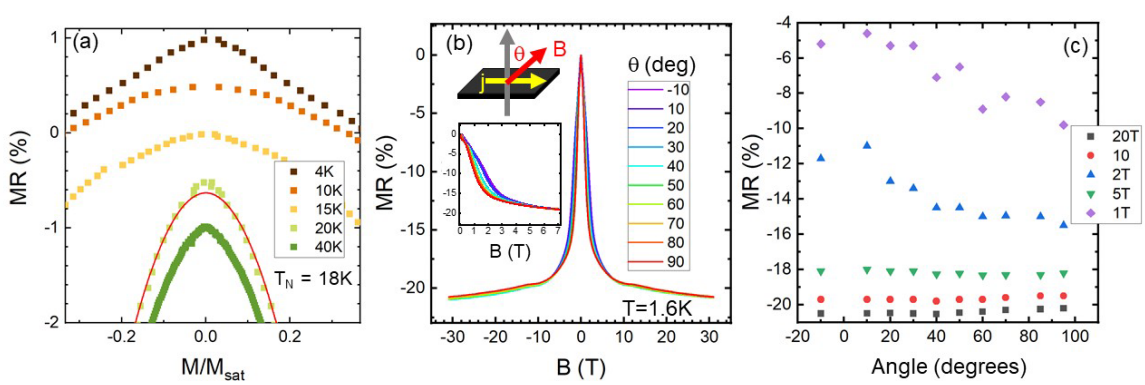

FIG. 4. (a) Scaling of the MR with magnetization relative to its saturation M/M_{sat} at different temperature. M_{sat} is the saturation magnetization at 4 K and 7 T. The curves are shifted for clarity. The solid red lines are parabolic curve fits. (b) Angular dependence of the magnetoresistance up to 31 T at $T = 1.6$ K. Insets: The direction of the magnetic field B with respect to the current, and graph of a zoom-in at low field (up to 7 T). (c) Magnetoresistance plotted as a function of angle for different values of magnetic field.

TABLE II. Magnetotransport characteristics compared to those from single crystals. $MR = [R(B)\text{-}R(0)]/R(0)$.

Source	Carrier density (cm^{-3})	Resistivity (mΩ-cm)	MR (%) at 3 T, 10 K
This work (t = 45 nm, 740 °C)	p = 7.5×10^{19}	1.19	–12.8
Ref. [10]	p = 6.5×10^{19}	–	–
Ref. [13]	–	0.4	–40
Ref. [6]	–	0.22	–50
Ref. [38]	–	0.32	–
Ref. [12]	p = 4.2×10^{19}	0.15	–10
Ref. [8]	p = 3.6×10^{20} (from R_H)	0.15	+5.6
Ref. [39]	p = 4.0×10^{19}	0.15	–
Ref. [15]	–	0.19	−10 (at 12 K)

phenomenon vastly different from the weak antilocalization (WAL) behavior expected for topological surface states in the diffusive regime. We did not see any evidence of WAL in the films studied here. But, future work on thinner films, thin enough to quantum confine the bulk bands (<20 nm), can potentially settle whether topological surface states with spin-momentum locking [10] contribute to magnetotransport in $EuIn_2As_2$. We also note that the colossal size of the magnetoresistance [in magnetoconductance ($\Delta G_{xx} \gg e^2/h$)] also rules out weak localization as a possible origin.

III. DISCUSSION

The transport characteristics of our films are compared to those found in previous studies on single crystals in Table II [38,39]. The charge carrier density is consistent with what is typical of $EuIn_2As_2$ and is within sample-to-sample variations found in single crystals. The magnitude of the negative MR measured at 3 T was smaller than what is reported in Refs. [6] and [13], but is also within sample-to-sample variations compared to prior work. The sample grown at 740 °C has the highest mobility; it reaches 70 cm^2/Vs. While this is too low to reach the Landau quantized regime at reasonable magnetic fields, it is consistent with previous work on single crystals (see Table II). The lowest resistivity was also measured in the sample grown at 740 °C. It is ten to four times larger than what was measured in single crystals.

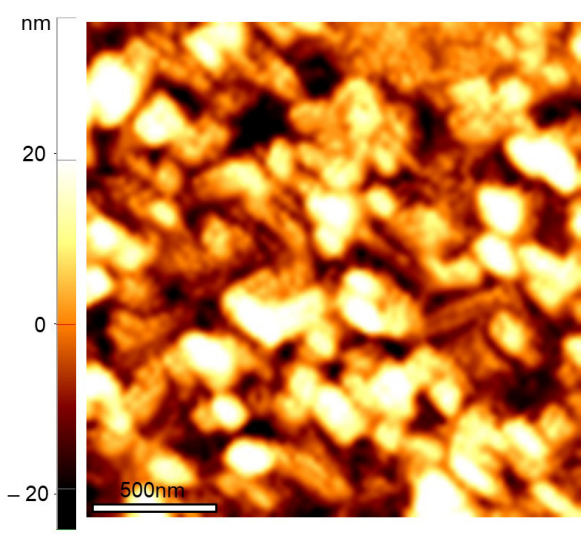

FIG. 5. Atomic force microscopy image of a 2-μm×2-μm area of the film grown at 740 °C.

Atomic force microscopy measurements shown in Fig. 5 shed light on discrepancies between films and single crystals. A surface roughness exceeding 10 nm, as seen in Fig. 5, accounts for the enhanced resistivity reported in Table II. The sample grown at 680 °C was not continuous, so its resistivity could not be measured. This indicates that a Stranski-Krastanov layer-plus-island process drives the nucleation of $EuIn_2As_2$ on lattice-mismatched sapphire. Additionally, this morphology can explain the broadening of the spin-flop transition [Fig. 2(c)] and the slight enhancement of magnetic field phase boundaries (B_{sf} and B_{sat}) compared to single crystals. The observed morphology can, in fact, lead to an inhomogeneous distribution of lattice and thermal strain, which can alter magnetic exchange interactions.

IV. CONCLUSION

We have successfully synthesized the Zintl phase of $EuIn_2As_2$ by MBE on sapphire. Our choice of substrate is primarily motivated by its ability to withstand a high substrate temperature during growth, which we found essential to stabilize the Zintl phase of $EuIn_2As_2$. The synthesis of $EuIn_2As_2$ on a lattice-matched substrate should be developed next to enhance the mobility further and reduce layer roughness. The films grown on sapphire reproduce the magnetic properties of bulk single crystals but yield a broadened spin-flop transition. The realization of thin films enables the application of a gate voltage to tune the Fermi level of $EuIn_2As_2$. It also opens the door to magnetooptical measurements at long wavelengths in the infrared, THz, and millimeter-wave parts of the spectrum [40–42]. Such measurements are needed to elucidate the magnetic field's impact on this material's band structure and to discover its predicted electrodynamic axion response.

ACKNOWLEDGMENTS

Work was supported by the National Science Foundation (Cooperative Agreement No. DMR-1905277). A portion of this work was performed at the National High Magnetic Field Laboratory, which is supported by the National Science Foundation (Cooperative Agreement No. DMR-2128556) and the State of Florida.

APPENDIX: NELSON RILEY ANALYSIS OF THE X-RAY DIFFRACTION PATTERN

The Nelson-Riley method allows us to determine the lattice parameter of $EuIn_2As$ with improved precision. We first compute the c lattice parameter using Bragg's law for each observed Bragg reflection [$(0\,0\,2n)$, $n = 2$ to 7]. We then plot all the values of c that we find against the Nelson-Riley function [43]:

$$f(\theta) = \tfrac{1}{2}[(\cos^2\theta)/\sin(\theta) + (\cos^2\theta)/\theta].$$

The plot is shown in Fig. 6. It yields $c = 17.874 \pm 0.003$ Å at the intercept between a linear fit to the data and the y-axis. This point represents the point for which various sources of uncertainty are minimized.

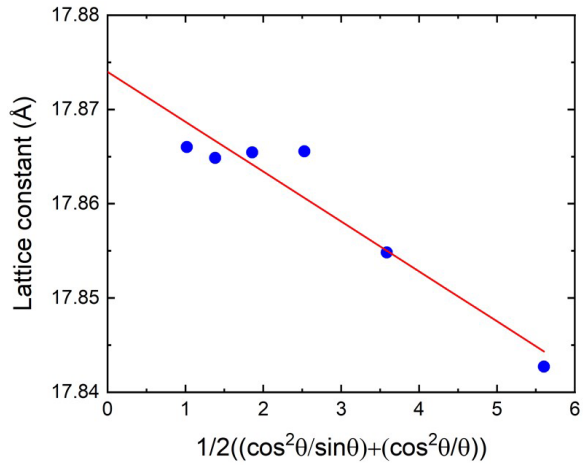

FIG. 6. Nelson-Riley analysis for the sample grown at 740 °C.

[1] C.- Z. Chang *et al.*, Experimental observation of the quantum anomalous Hall effect in a magnetic topological insulator, Science **340**, 167 (2013).

[2] Y. Tokura, K. Yasuda, and A. Tsukazaki, Magnetic topological insulators, Nat. Rev. Phys. **1**, 126 (2019).

[3] N. P. Armitage, E. J. Mele, and A. Vishwanath, Weyl and Dirac semimetals in three-dimensional solids, Rev. Mod. Phys. **90**, 015001 (2018).

[4] C.-Z. Chang, C.-X. Liu, and A. H. MacDonald, *Colloquium*: Quantum anomalous Hall effect, Rev. Mod. Phys. **95**, 011002 (2023).

[5] C.-Z. Chang, P. Wei, and J. S. Moodera, Breaking time reversal symmetry in topological insulators, MRS Bull. **39**, 867 (2014).

[6] A. M. Goforth, P. Klavins, J. C. Fettinger, and S. M. Kauzlarich, Magnetic properties and negative colossal magnetoresistance of the rare earth Zintl phase $EuIn_2As_2$, Inorg. Chem. **47**, 11048 (2008).

[7] Y. Xu, Z. Song, Z. Wang, H. Weng, and X. Dai, Higher-order topology of the axion insulator $EuIn_2As_2$, Phys. Rev. Lett. **122**, 256402 (2019).

[8] Y. Zhang, K. Deng, X. Zhang, M. Wang, Y. Wang, C. Liu, J.- W. Mei, S. Kumar, E. F. Schwier, K. Shimada, C. Chen, and B. Shen, In-plane antiferromagnetic moments and magnetic polaron in the axion topological insulator candidate $EuIn_2As_2$, Phys. Rev. B **101**, 205126 (2020).

[9] S. X. M. Riberolles, T. V. Trevisan, B. Kuthanazhi, T. W. Heitmann, F. Ye, D. C. Johnston, S. L. Bud'ko, D. H. Ryan, P. C. Canfield, A. Kreyssig, A. Vishwanath, R. J. McQueeney, L. L. Wang, P. P. Orth, and B. G. Ueland, Magnetic crystalline-symmetry-protected axion electrodynamics and field-tunable unpinned Dirac cones in $EuIn_2As_2$, Nat. Commun. **12**, 999 (2021).

[10] T. Sato, Z. Wang, D. Takane, S. Souma, C. Cui, Y. Li, K. Nakayama, T. Kawakami, Y. Kubota, C. Cacho, T. K. Kim, A. Arab, V. N. Strocov, Y. Yao, and T. Takahashi, Signature of band inversion in the antiferromagnetic phase of axion insulator candidate $EuIn_2As_2$, Phys. Rev. Res. **2**, 033342 (2020).

[11] S. Regmi, M. M. Hosen, B. Ghosh, B. Singh, G. Dhakal, C. Sims, B. Wang, F. Kabir, K. Dimitri, Y. Liu, A. Agarwal, H. Lin, D. Kaczorowski, A. Bansil, and M. Neupane, Temperature-dependent electronic structure in a higher-order topological insulator candidate $EuIn_2As_2$, Phys. Rev. B **102**, 165153 (2020).

[12] J. Yan, Z. Z. Jiang, R. C. Xiao, W. J. Lu, W. H. Song, X. B. Zhu, X. Luo, Y. P. Sun, and M. Yamashita, Field-induced topological Hall effect in antiferromagnetic axion insulator candidate EuIn temperature-dependent electronic structure in a higher-order topological insulator candidate $EuIn_2As_2$, Phys. Rev. Res. **4**, 013163 (2022).

[13] F. H. Yu, H. M. Mu, W. Z. Zhuo, Z. Y. Wang, Z. F. Wang, J. J. Ying, and X. H. Chen, Elevating the magnetic exchange coupling in the compressed antiferromagnetic axion insulator candidate $EuIn_2As_2$, Phys. Rev. B **102**, 180404(R) (2020).

[14] S. M. Kauzlarich, A. Zevalkink, E. Toberer, and G. J. Snyder, in *Thermoelectric Materials and Devices*, edited by I. Nandhakumar, N. M. White, and S. Beeby (The Royal Society of Chemistry, London, 2016), pp. 1–26.

[15] T. Tolinski and D. Kaczorowski, Magnetic properties of the putative higher-order topological $EuIn_2As_2$, SciPost Phys. Proc. **11**, 005 (2022).

[16] J. Jiang and S. M. Kauzlarich, Colossal magnetoresistance in a rare earth Zintl compound with a new structure type: $EuIn_2P_2$, Chem. Mater. **18**, 435 (2006).

[17] S. Von Molnar and S. Methfessel, Giant negative magnetoresistance in ferromagnetic Eu1-xGdxSe, J. Appl. Phys. **38**, 959 (1967).

[18] S. Von Molnar, J. M. Tarascon, and J. Etourneau, Transport and magnetic properties of carbon doped EuB_6, J. Appl. Phys. **52**, 2158 (1981).

[19] A. M. Essin, J. E. Moore, and D. Vanderbilt, Magnetoelectric polarizability and axion electrodynamics in crystalline insulators, Phys. Rev. Lett. **102**, 146805 (2009).

[20] J. Ahn, S. Y. Xu, and A. Vishwanath, Theory of optical axion electrodynamics and application to the Kerr effect in topological antiferromagnets, Nat. Commun. **13**, 7615 (2022).

[21] M. Yano, M. Nogami, Y. Matsushima, and M. Kimata, Molecular beam epitaxial growth of InAs, Jpn. J. Appl. Phys. **16**, 2131 (1977).

[22] P. F. S. Rosa, C. Adriano, T. M. Garitezi, R. A. Ribeiro, Z. Fisk, and P. G. Pagliuso, Electron spin resonance of the intermetallic antiferromagnet $EuIn_2As_2$, Phys. Rev. B **86**, 094408 (2012).

[23] S. Foner, High-field antiferromagnetic resonance in Cr_2O_3, Phys. Rev. **130**, 183 (1963).

[24] I. S. Jacobs, Spin-flopping in MnF_2 by high magnetic fields, J. Appl. Phys. **32**, S61 (1961).

[25] J. Coey, *Magnetism and Magnetic Materials* (Cambridge University Press, Cambridge, 2010).

[26] O. Caha, A. Dubroka, J. Humlíčk, V. Holy, H. Steiner, M. Ul-Hassan, J. Sánchez-Barriga, O. Rader, T. N. Stanislavchuk, A. A. Sirenko, G. Bauer, and G. Springholz, Growth, structure, and electronic properties of epitaxial bismuth telluride topological insulator films on BaF_2 (111) substrates, Cryst. Growth Des. **2**, 3365 (2013).

[27] N. Peranio, M. Winkler, M. Dürrschnabel, J. König, and O. Eibl, Assessing antisite defect and impurity concentrations in Bi_2Te_3 based thin films by high-accuracy chemical analysis, Adv. Funct. Mater. **23**, 4969 (2013).

[28] B. A. Assaf, T. Cardinal, P. Wei, F. Katmis, J. S. Moodera, and D. Heiman, Linear magnetoresistance in topological insulator thin films: Quantum phase coherence effects at high temperatures, Appl. Phys. Lett. **102**, 012102 (2013).

[29] J. B. Torrance, M. W. Shafer, and T. R. McGuire, Bound magnetic polarons and the insulator-metal transition in EuO, Phys. Rev. Lett. **29**, 1168 (1972).

[30] M. Pohlit, S. Rößler, Y. Ohno, H. Ohno, S. von Molnár, Z. Fisk, J. Müller, and S. Wirth, Evidence for ferromagnetic clusters in the colossal-magnetoresistance material EuB, Phys. Rev. Lett. **120**, 257201 (2018).

[31] G. Weill, I. A. Smirnov, and V. N. Gurin, Pressure measurements of electrical transport properties of EuB_6, J. Phys. Colloq. **41**, C5-185 (1980).

[32] A. M. Goforth, H. Hope, C. L. Condron, S. M. Kauzlarich, N. Jensen, P. Klavins, S. MaQuilon, and Z. Fisk, Magnetism and negative magnetoresistance of two magnetically ordering, rare-earth-containing Zintl phases with a new structure type: $EuGa_2Pn_2$ (Pn = P, As), Chem. Mater. **21**, 4480 (2009).

[33] F. Pfuner, L. Degiorgi, H.-R. Ott, A. Bianchi, and Z. Fisk, Magneto-optical behavior of $EuIn_2P_2$, Phys. Rev. B **77**, 024417 (2008).

[34] P. Majumdar and P. B. Littlewood, Dependence of magnetoresistivity on charge-carrier density in metallic ferromagnets and doped magnetic semiconductors, Nature (London) **395**, 479 (1998).

[35] P. Rosa, Y. Xu, M. Rahn, J. Souza, S. Kushwaha, L. Veiga, A. Bombardi, S. Thomas, M. Janoschek, E. Bauer, M. Chan, Z. Wang, J. Thompson, N. Harrison, P. Pagliuso, A. Bernevig, and F. Ronning, Colossal magnetoresistance in a nonsymmorphic antiferromagnetic insulator, npj Quantum Mater. **5**, 52 (2020).

[36] B. A. Assaf, T. Phuphachong, E. Kampert, V. V. Volobuev, P. S. Mandal, J. Sánchez-Barriga, O. Rader, G. Bauer, G. Springholz, L. A. De Vaulchier, and Y. Guldner, Negative longitudinal magnetoresistance from the anomalous $N = 0$ landau level in topological materials, Phys. Rev. Lett. **119**, 106602 (2017).

[37] X. Dai, Z. Z. Du, and H.-Z. Lu, Negative magnetoresistance without chiral anomaly in topological insulators, Phys. Rev. Lett. **119**, 166601 (2017).

[38] B. Xu, P. Marsik, S. Sarkar, F. Lyzwa, Y. Zhang, B. Shen, and C. Bernhard, Infrared study of the interplay of charge, spin, and lattice excitations in the magnetic topological insulator $EuIn_2As_2$, Phys. Rev. B **103**, 245101 (2021).

[39] K. Shinozaki, Y. Goto, K. Hoshi, R. Kiyama, N. Nakamura, A. Miura, C. Moriyoshi, Y. Kuroiwa, H. Usui, and Y. Mizuguchi, Thermoelectric properties of the As/P-based Zintl compounds $EuIn_2As_{2-x}P_x (x = 0–2)$ and $SrSn_2As_2$, ACS Appl. Energy Mater. **4**, 5155 (2021).

[40] L. Wu, M. Salehi, N. Koirala, J. Moon, S. Oh, and N. P. Armitage, Quantized Faraday and Kerr rotation and axion electrodynamics of a 3D topological insulator, Science **354**, 1124 (2016).

[41] J. Wang, X. Liu, T. Wang, M. Ozerov, and B. A. Assaf, *g* factor of topological interface states in $Pb_{1-x}Sn_xSe$ quantum wells, Phys. Rev. B **107**, 155307 (2023).

[42] J. Wang, T. Wang, M. Ozerov, Z. Zhang, J. Bermejo-Ortiz, S.-K. Bac, H. Trinh, M. Zhukovskyi, T. Orlova, H. Ambaye, J. Keum, L.-A. de Vaulchier, Y. Guldner, D. Smirnov, V. Lauter, X. Liu, and B. A. Assaf, Energy gap of topological surface states in proximity to a magnetic insulator, Commun. Phys. **6**, 200 (2023).

[43] J. B. Nelson and D. P. Riley, An experimental investigation of extrapolation methods in the derivation of accurate unit-cell dimensions of crystals, Proc. Phys. Soc. **57**, 160 (1945).